Magnetic voltage isolator for the feedback loop of power converters for space applications

J. Antonio Fernández[1], Abraham López[1], Theyllor H. Oliveira[1], Pablo F. Miaja[1], Manuel Arias[1], Arturo Fernández[2]
1 Power Supply Group (Universidad de Oviedo). Gijón, Spain
2 European Space Agency (ESA) - ESTEC. Noordwijk, Netherlands
fernandezalvantonio@uniovi.es

***Abstract*—Optocouplers are among the components most adversely affected by space radiation, resulting in diminished performance and a shortened lifespan. This article presents a device, based on a current-fed Push-Pull topology DC/DC converter, designed to isolate the feedback loop signal of a power converter. Furthermore, a mathematical model has been developed, playing a pivotal role in the study. This model facilitates the identification of nonlinearities within the system, ensures precise knowledge of the current transfer ratio, and serves as a design guide to achieve accurate behavior. Python was utilized for evaluating the mathematical model, while PSIM was employed for assessing the system circuit, thus presenting experimental results as well.**

***Index Terms*—DC/DC Converters, power electronics, space, feedback, isolators.**

I. Introduction

Optocouplers are critical components in space power systems due to the degradation caused by space radiation, which reduces their performance and shortens their lifespan [1], [2], [3]. The current transfer ratio is the primary parameter affected by this radiation and is a key metric in the feedback loop of isolated DC/DC converters. While various solutions exist on the market, most are not qualified for space systems [4]. This qualification process is highly complex, costly, and time-consuming. Although some space-qualified solutions are available, they are often expensive and have limited bandwidth [5], [6], [7]. To address this issue, an alternative solution based on a Push-Pull topology DC/DC converter has been developed. This device, constructed with space-qualified components, provides the same functionality as an optocoupler and offers a dynamic response comparable to that of currently available space-qualified devices.

The device designed is developed to be connected on the feedback loop. For that reason, a set of requirements has been set to define the development of the device:

- Isolation voltage similar to optocouplers.
- Output voltage should be same as input voltage.
- Provide dynamic behavior according to equivalent isolator devices present on the market.

II. Model proposed

To ensure the proper functioning within the feedback loop of the converters, the proposed device must provide an output voltage proportional to the input voltage across the entire range of the latter voltages. This implies a linear gain in the device, which is reflected in a flat frequency response across the isolator's entire bandwidth. Rectification stage on DC/DC transformers can present a significant issue, mostly on low-voltage applications, like the proposed on this project. If this rectification is performed using diodes, there will be a voltage difference caused by the voltage drop at the diodes. This voltage drop is mainly dictated by the knee voltage, which strongly depends on the temperature. To overcome this problem, the proposed isolator first converts the input voltage into a current and transfers it through the transformer and the rectifier diodes, because the current is not affected by the changes in the voltage drop. Therefore, a current-fed Push-Pull topology has been implemented. This topology has been selected since the transformer driver switches are referred to ground, easing the driving of the switches.

Figure 1 presents a block diagram of the system proposed, depicting the main stages of the device. The first stage involves generating the current to be transferred. An operational amplifier is used (which also acts as an impedance decoupler) along with a transistor and a resistance. This is followed by a current mirror stage that functions as a constant current source to feed the Push-Pull transformer. The next stage involves isolation, consisting of a magnetic transformer, an analog oscillator which controls the converter switches, and a rectification stage with four diodes. After rectification, the current passes through a Current-to-Voltage conversion stage implemented by a second set of current mirrors. In addition to converting the current to voltage, the first mirror limits the voltage on the Push-Pull converter's magnetic transformer, while the second changes the direction of the current, channeling it towards the resistor where the output voltage will be generated. In the final stage, an operational amplifier acts as an impedance decoupler and regulates the gain as necessary.

For the Voltage-Current and Current-Voltage conversion stages, Wilson current mirrors have been utilized. This topology offers high precision in V-I conversion, which is crucial for this application [8]. Additionally, to achieve a compact magnetic transformer size while ensuring good dynamic performance, the system must operate at the highest possible switching frequency. The high bandwidth of the selected current mirrors and operational amplifiers means that the isolator's bandwidth is constrained by the switching frequency

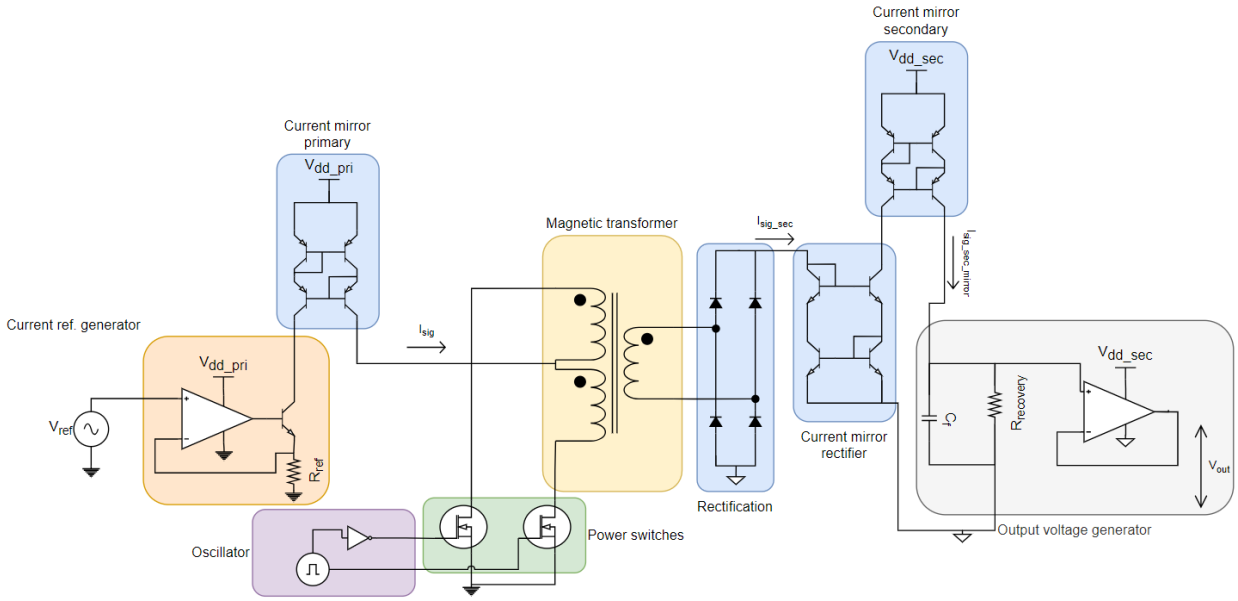

Fig. 1. Model proposed circuit.

of the Push-Pull converter stage. Specifically, the oscillator and switch components limit this switching frequency to approximately 4 MHz.

III. Gain and Linearity Analysis

The initial point of the analysis involves validating the Wilson mirrors and the current generator stages. A range of voltages has been measured, utilizing different resistance values for R_{ref}. After conducting various tests where different currents were injected, it was observed that these stages did not affect the linearity of the transferred current, and the voltage measured at the output was the same as the sensed at the input. This indicates that the critical design point of the device lies in the current-fed Push-Pull transformer stage. Aiming to switch at high frequencies, Figure 2 shows the circuit diagram modeling the switching process. This diagram makes used of the T equivalent of the transformer presented in [9], which considers all components that significantly impact the device's gain and linearity, primarily the parasitic capacitances.

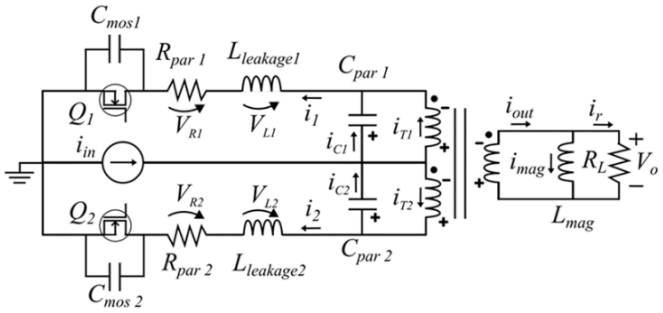

Fig. 2. Equivalent circuit for switching process analysis.

An important aspect of the system design is ensuring that the current transferred through the transformer is not interrupted. Interruption of the current during the switching process will make the output transistors of the primary current mirror go into saturation. In order to act as a current source the transistors of the current mirror need to remain in active zone. To prevent this, the duty cycle of the control signal for the switches must always be greater than 0.5. This ensures that both switches are closed simultaneously, allowing current to flow through both windings and generate opposing magnetic fields that prevent current transference to the secondary during this period. This phenomenon is illustrated in Figure 3.

Due to the high switching frequency, the impact of this non-transferred current is significant. Additionally, the charging and discharging times of parasitic capacitances significantly affect the gain of the current transference. Therefore, a detailed mathematical analysis has been conducted to quantify this influence in order to take it into account in the design for achieving a desired gain between input and output voltages.

Focusing on Figure 3, there are two main stages to analyze: the moment when a switch closes, allowing current to flow through both windings (Stage 1), and the moment when the other switch opens (Stage 2). The mathematical analysis requires the following assumptions:

- The parasitic components of the upper winding (indicated with the subscript 1) are equal to those of the lower winding (indicated with the subscript 2).
- Leakage Inductance is represented in upper and lower windings because most of the time only one of them is conducting.
- The transformer's parasitic capacitance only affects the circuit during Stage 2, as observed from simulations conducted with PSIM software.

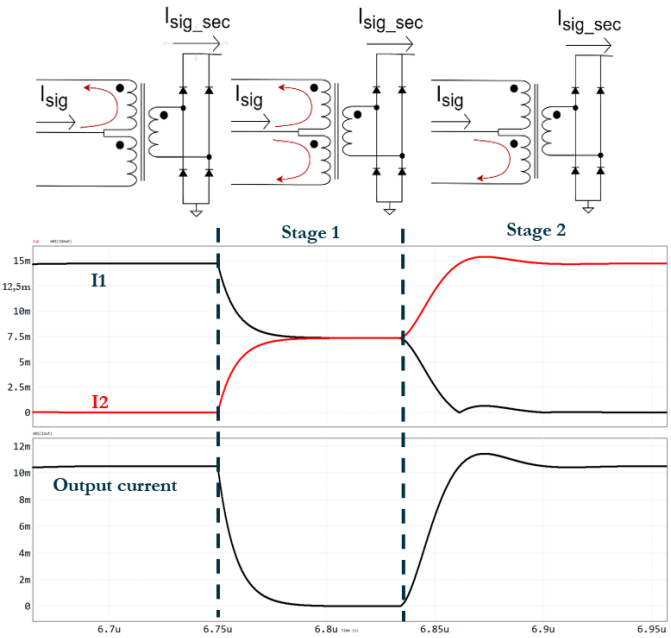

Fig. 3. Switching process currents.

A. Stage 1 analysis

In this state, the parasitic capacitances of the switches have no effect on the circuit, as they are short-circuited when the switches are closed. The equations that model the circuit in Figure 2 are:

$$I_{\text{in}} = I_{T1} + I_{T2} \tag{1}$$

$$I_{\text{in}} = I_1 + I_2 \tag{2}$$

$$I_1 = C_p \cdot \frac{dV_o(t)}{dt} + I_{T1} \tag{3}$$

$$I_2 = -C_p \cdot \frac{dV_o(t)}{dt} + I_{T2} \tag{4}$$

$$\frac{V_o}{R_o} = I_{T1} - I_{T2} \tag{5}$$

$$2V_o + V_{L1} + V_{R1} = V_{L2} + V_{R2} \tag{6}$$

Which contains the following 5 variables:

$$I_{T1}, I_{T2}, I_1, I_2, V_o$$

These equations lead to the following second-order differential equation:

$$LC_p \frac{d^2V_o(t)}{dt^2} + \left(\frac{L}{2R_L} + R_pC_p\right)\frac{dV_o(t)}{dt} + \left(1 + \frac{R_p}{2R_L}\right)V_o(t) = 0 \tag{7}$$

The solution to this equation is neither straightforward nor simple, as the values of the components determine the type of response the circuit will exhibit: underdamped, overdamped, or critically damped. The first step is to obtain the roots of the equation:

$$r = \frac{-b \pm \sqrt{b^2 - 4ac}}{2a} \tag{8}$$

Using the values of (7) in (8) yields:

$$r = \frac{-1}{4R_LC_p} \pm \sqrt{\frac{(L - 16R_L^2C_p)}{16R_L^2C_p^2L}} \tag{9}$$

The response of the system is determined by the discriminant of (9):

$$\frac{(L - 16R_L^2C_p)}{16R_L^2C_p^2L} \tag{10}$$

For each type of response, the particular solution for $V_o(t)$ is:

- Overdamped:

$$V_o(t) = K_1e^{r_1t} + K_2e^{r_2t} \tag{11}$$

- Underdamped:

$$V_o = e^{-at}(K_1\cos(bt) + K_2\sin(bt)) \tag{12}$$

- Critically damped:

$$V_o(t) = (K_1 + K_2t)e^{rt} \tag{13}$$

It can be observed that in each scenario, two unknowns (K1 and K2) are present. To solve for these, a second equation is required, which defines the current through the parasitic capacitance in the transformer:

$$I_{c1}(t) = C_p \cdot \frac{dV_o(t)}{dt} \tag{14}$$

To solve them, it is necessary to know the initial conditions of the circuit. At the moment of switching (t=0), the output current is equal to the input current multiplied by the transformer ration. Also, the parasitic capacitance of the transformer will be fully charged, hence no current is passing through the capacitor:

$$V_o(0) = R_L \cdot I_{in} \tag{15}$$

$$I_{c1}(0) = 0 \tag{16}$$

Table 1 presents the resolved equations used to determine the output current of the secondary winding of the transformer. These equations are based on the values of the parasitic components of the various devices that compose the system and the input current of the transformer. The frequency value does not influence this section, as the objective is to observe the temporal evolution during the moment the switch is closed.

To evaluate this equation and observe the curve generated, python has been used. The values of the components have been obtained from the datasheets of the devices utilized in the prototype exposed on V. Figure 4 represents the curve generated for the winding currents, where it can be seen how both converge to half the value of the input current. Figure 5 represents the output current dropping to 0 A and maintain it during both switches are closed.

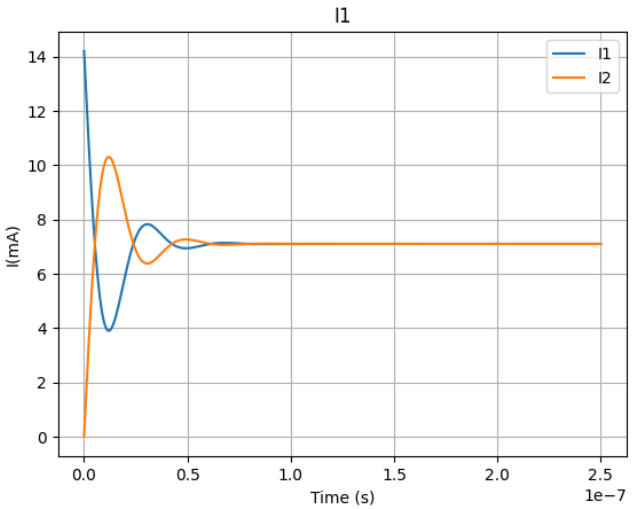

Fig. 4. Stage 1 winding currents

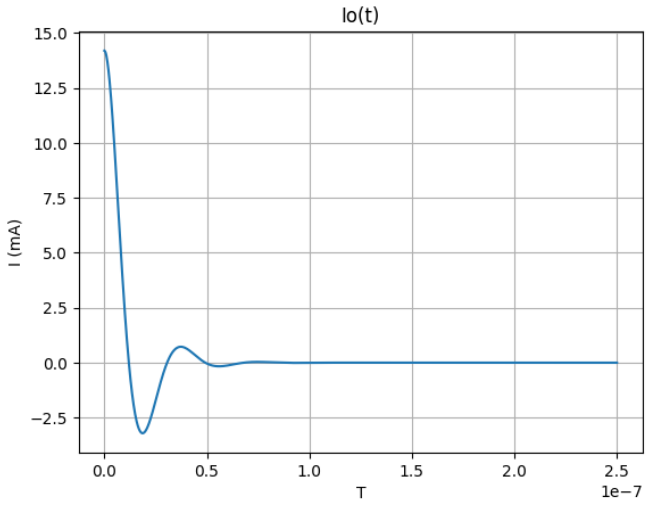

Fig. 5. Stage 1 output current

B. Stage 2 analysis

The parasitic capacitance of the switches have effect on this stage, while the parasitic capacitance of the transformer can be omitted for these calculations. The equations that model the behavior of the circuit in Figure 2 are:

$$I_2 = I_{in} - I_1 \tag{17}$$

$$I_{out} = 2I_1 - I_{in} \tag{18}$$

$$I_1 = C_m \cdot \frac{dV_c(t)}{dt} \tag{19}$$

$$2I_{out}R_L + L\frac{dI_1(t)}{dt} + I_1(t)R_p + V_c = L\frac{dI_2(t)}{dt} + I_2(t)R_p \tag{20}$$

Which contains the following variables:

$$I_{out}, V_c, I_1, I_2$$

These equations lead to the following second-order differential equation:

$$2LC_m\frac{d^2V_c(t)}{dt^2} + 4R_LC_m\frac{dV_c(t)}{dt} + V_c(t) = 2R_LI_{in} \tag{21}$$

The procedure for solving this equation differs from the previous stage because the resulting equation has a non-zero independent term. The solution for a non-homogeneous differential equation is expressed as:

$$V_c(t) = V_{c_g}(t) + V_{c_p}(t) \tag{22}$$

$V_{cp}(t)$ corresponds to the particular solution of the equation. Since the independent component of the equation is constant, $V_c(t)$ can also be assumed to be constant. Thus, its respective derivatives would be 0, and the particular solution is expressed as:

$$V_{c_p}(t) = 2R_LI_{in} \tag{23}$$

$V_{c_p}(t)$ is the solution to the homogeneous equivalent equation:

$$2LC_m\frac{d^2V_c(t)}{dt^2} + 4R_LC_m\frac{dV_c(t)}{dt} + V_c(t) = 0 \tag{24}$$

The solution to (24) will be similar to (7). The roots have to be obtained and the response of the system is determined by the discriminant of (25):

$$r = \frac{-R_L}{L} \pm \sqrt{\frac{2R_L^2C_m - L}{2C_mL^2}} \tag{25}$$

The particular solutions for the equivalent homogeneous equation are the same as those expressed in (11), (12), and (13), but applied to $V_c(t)$. As in the previous case, each response involves two unknowns (K1 and K2). To find them, a second equation is needed: the current through the parasitic capacitance of the switch.

$$I_1(t) = C_m \cdot \frac{dV_c(t)}{dt} \tag{26}$$

Regarding the initial conditions of the voltage $V_c(t)$, the switch is closed and short-circuited at the initial instant. On the other side, the current through the switch I_1 during that moment is half of the input current, as it is divided between the two windings.

$$V_c(0) = 0 \tag{27}$$

$$I_1(0) = \frac{I_{in}}{2} \tag{28}$$

Table 1 shows the equation defining the output current in this stage, derived from solving the current equation I_1 and (18). As it has been shown on the Stage 1 evaluation, python has been used to evaluate these expressions. Figure 6 represents the currents through the windings. Figure 7 represents the output current reaching the input current value and maintain it during the rest of the period.

TABLE I
OUTPUT CURRENT EQUATIONS

	I_{out}	***Roots***	***K constants***
Stage 1			
Overdamped	$I_o(t) = \frac{1}{R_L}\left(K_1 e^{r_1 t} + K_2 e^{r_2 t}\right)$	$r_{1,2} = \frac{-1}{4R_L C_p} \pm \sqrt{\frac{L-16R_L^2 C_p}{16R_L^2 C_p^2 L}}$	$K_1 = \frac{r_2 I_{\text{in}} R_L}{r_2 - r_1}$ $K_2 = \frac{r_1 I_{\text{in}} R_L}{r_1 - r_2}$
Underdamped	$I_o(t) = \frac{1}{R_L} e^{-at}\left(K_1 \cos(bt) + K_2 \sin(bt)\right)$	$a = \frac{1}{4R_L C_p}, \quad b = \sqrt{\frac{16R_L^2 C_p - L}{16R_L^2 C_p^2 L}}$	$K_1 = I_{\text{in}} R_L$ $K_2 = \frac{a}{b} I_{\text{in}} R_L$
Critically Damped	$I_o(t) = \frac{1}{R_L}(K_1 + K_2 t)e^{rt}$	$r = \frac{1}{4R_L C_p}$	$K_1 = I_{\text{in}} R_L$ $K_2 = -r I_{\text{in}} R_L$
Stage 2			
	I_{out}	***Roots***	***K constants***
Overdamped	$I_o(t) = 2C_m(r_1 K_1 e^{r_1 t} + r_2 K_2 e^{r_2 t}) - I_{\text{in}}$	$r_{1/2} = -\frac{R_L}{L} \pm \sqrt{\frac{2R_L^2 C_m - L}{2C_m L^2}}$	$K_1 = \frac{I_{in}/2C_m + r_2 2R_L I_{\text{in}}}{r_1 - r_2}$ $K_2 = \frac{I_{in}/2C_m + r_1 2R_L I_{\text{in}}}{r_2 - r_1}$
Underdamped	$I_o(t) =$ $2C_m\left(-ae^{-at}\left(K_1\cos(bt) + K_2\sin(bt)\right)\right.$ $\left.+e^{-at}\left(-bK_1\sin(bt) + bK_2\cos(bt)\right)\right) - I_{\text{in}}$	$a = -\frac{R_L}{L}, \quad b = \sqrt{\frac{-(2R_L^2 C_m - L)}{2C_m L^2}}$	$K_1 = -2R_L I_{\text{in}}$ $K_2 = \frac{I_{\text{in}}/2 - aC_m 2R_L I_{\text{in}}}{bC_m}$
Critically damped	$I_o(t) = 2C_m\left(K_2 e^{rt} + (K_1 + K_2 t)re^{rt}\right) - I_{\text{in}}$	$r = -\frac{R_L}{L}$	$K_1 = -2R_L I_{\text{in}}$ $K_2 = \frac{I_{\text{in}}}{2C_m} + 2R_L I_{\text{in}} r$

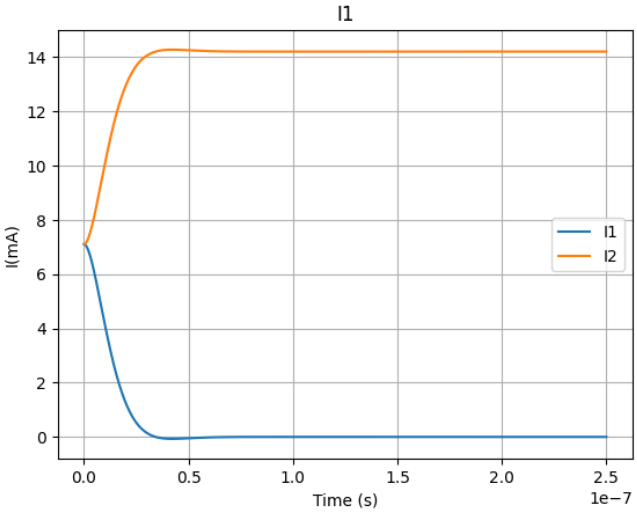

Fig. 6. Stage 2 winding currents

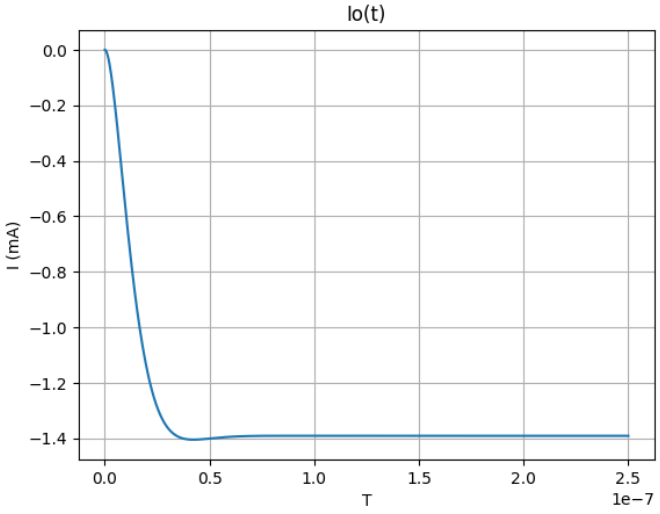

Fig. 7. Stage 2 output current

C. Magnetizing Inductance analysis

The lack of current transference between primary and secondary during switch overlap represents a challenge encountered in developing this device, though not the only one. Additionally, the necessity of minimizing transformer size implies a resultant magnetizing inductance that must also be minimized. This parameter warrants critical attention because insufficient magnetizing inductance can cause the magnetizing current to approach the level of the input current, thereby hindering its transfer to the secondary winding. This phenomenon is illustrated in Figure 8. Upper side of the image represents the desire behavior of the system, while the lower side exemplifies when the magnetizing inductance is lower than the desired value. It is represented how the current transferred (I_{tx}) is lower than the input current (I_{in}).

To calculate the minimum required inductance value necessary to mitigate this issue, it must start with the equation governing the voltage drop across an inductor (29):

$$V_{\text{mag}} = L_m \frac{dI_{Lm}}{dt} \tag{29}$$

$$L_{\text{mag}} = \frac{t_{\text{on}} \cdot V_{\text{mag}}}{\Delta I_{Lm}} \tag{30}$$

T_on refers to the time interval during which the magnetic flux increases, specifically half of the period.

$$t_{\text{on}} = \frac{T}{2} = \frac{1}{2 \cdot f} \tag{31}$$

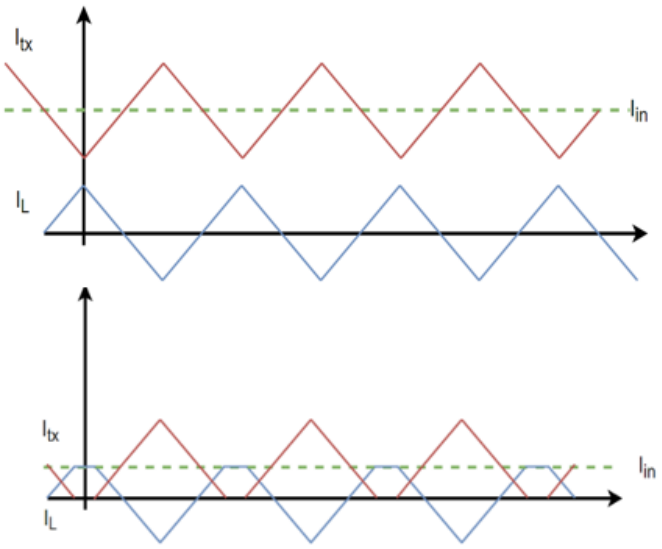

Fig. 8. Magnetizing inductance current.

To ensure that the magnetizing current does not reach the value of the input current, it must be ensured that:

$$i_{in} > \frac{\Delta I_{Lm}}{2} \tag{32}$$

Combining (30), (31), and (32) yields the following expression that limits the design of the magnetic transformer for our application:

$$L_{\text{mag}} > \frac{V_{\text{mag}}}{2 \cdot f \cdot 2 \cdot i_{in}} \tag{33}$$

That expression can be posted as the minimum current that a transformer with a fixed magnetizing inductance can give:

$$i_{in} > \frac{V_{\text{mag}}}{2 \cdot f \cdot 2 \cdot L_{\text{mag}}} \tag{34}$$

IV. Simulation

To analyze the complete switching cycle of the device in detail, it is essential to employ mathematical analysis tools. In this project, Python has been utilized through the Jupyter Notebooks interface. Knowledge of the switching frequency and the duty cycle of the signal is required to accurately analyze the equations describing the output current and obtain its average value, to see the non-transference of the current. The duty cycle provides the overlapping time between switches.

To validate this mathematical model and analyze each stage independently, the circuit analysis tool PSIM has been employed to simulate the circuit depicted in Figure 2. The parasitic components data used for the equations and for the PSIM circuit were obtained from the component datasheets used in the prototype exposed on Section V. Regarding the magnetic transformer, a unit from Coilcraft was utilized, featuring a 1:1.4 turns ratio. An impedance analyzer has been used for a precise transformer characterization of its magnetic and leakage inductance values. Figure 9 illustrates the output current waveform in both PSIM and Python for an input current of 1.4 mA, a switching frequency of 2 MHz, and a 51% duty cycle.

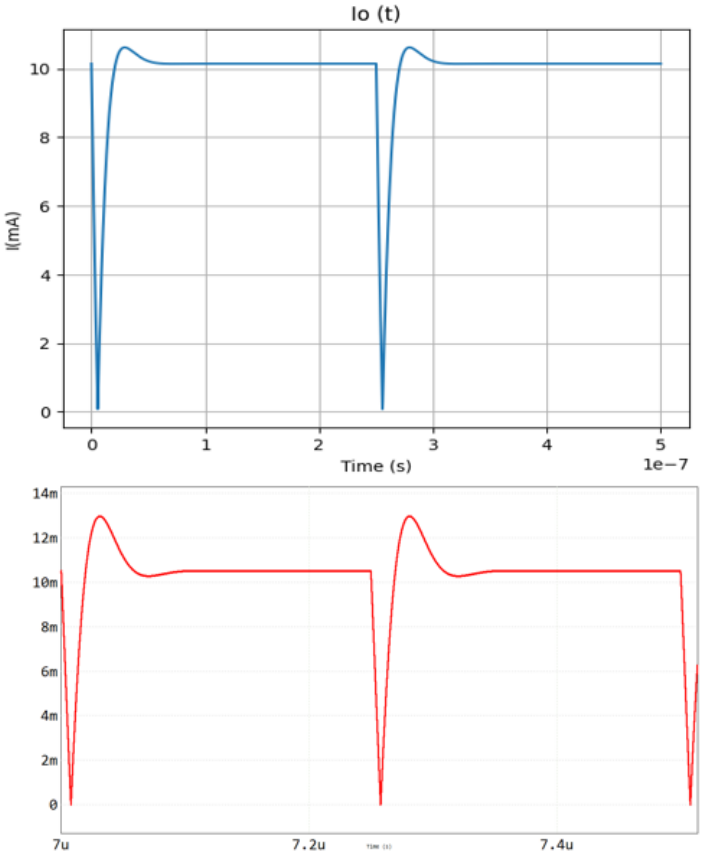

Fig. 9. Sim Math - Underdamped comparison.

A range of currents has been processed to see simulation and mathematical models current transfer gain, and differences between the two models. Table II shows a series of input current and the output current value obtained on the Mathematical model and on the simulated one in PSIM. Figure 10 illustrates the outputs values, where the linearity of the current transfer gain can be observed.

TABLE II
Comparison of Current Values

i_{in} (mA)	PSIM (mA)	Math (mA)
8.90	6.17	6.17
10.70	7.42	7.41
12.50	8.66	8.67
14.20	9.84	9.85
16.00	11.10	11.09
17.80	12.34	12.34
19.60	13.58	13.59
21.40	14.83	14.82

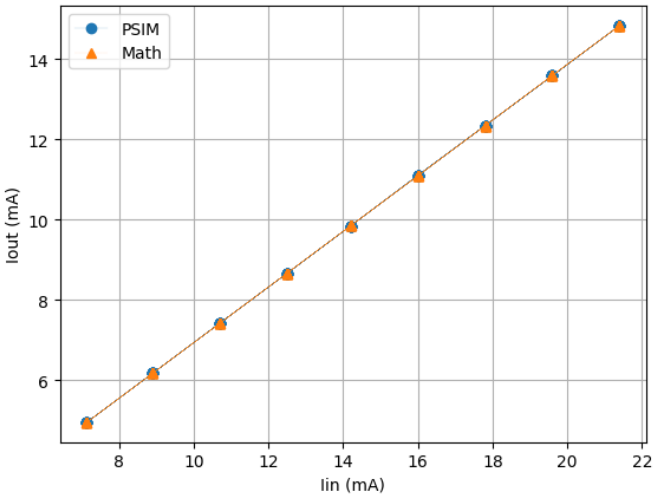

Fig. 10. Mathematical model and simulation comparison.

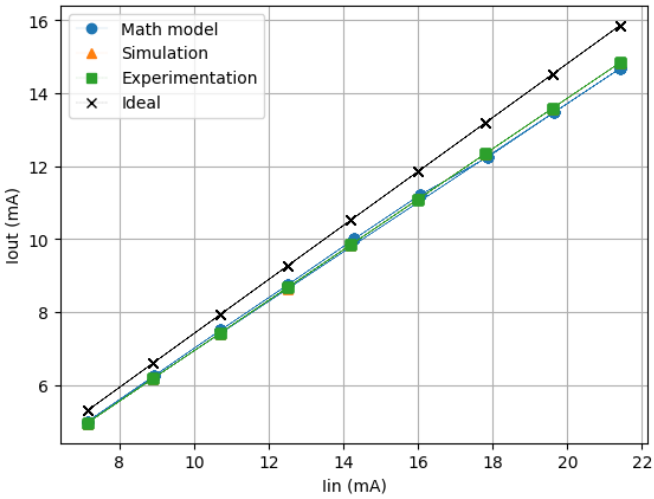

Fig. 12. Math model, simulation and PSIM comparative

V. Experimentation

For this project, a prototype was constructed using space-qualified components. Figure 11 exposes this device developed.

Fig. 11. Prototype developed

A transformer from Coilcraft was selected for this prototype, which has been exposed on Section IV. One of the critical studies carried out on the prototype was to operate at the boundary duty cycle (51%), with a switching frequency of 2 MHz, feeding the transformer with a current of 14 mA. The purpose of the test is to evaluate if the simulation and mathematical model can replicate the behavior of the prototype. The target is to observe the voltage across a resistance connected to the transformer secondary winding to evaluate the current reaching the output.

Figure 12 presents a comparison between the experimental results, the PSIM simulation, the mathematical model, and the ideal output of the device (the input current attenuated by a factor of 1.4) for a switching frequency of 2 MHz and a duty cycle of 50%. The ideal output is defined by the transformer transfer ratio, which does not account for the phenomena described by the mathematical model. Meanwhile, it can be observed that the actual (experimental) output exhibits a significant gain and voltage difference compared to the ideal output. This highlight the necessity of modeling the device attenuation which, in addition with the simulation model, fits accurately with the experimental results, offering a guidance to detect these derivations and a precise design guide.

VI. Conclusions

A magnetic isolator capable of replacing optocouplers has been successfully developed using space-qualified components. Additionally, a comprehensive mathematical model of the system has been created, which accurately identifies the influence of all parasitic components and highlights the weak points. This model allows for precise control over the device design, facilitating the accurate replication of the complex behavior of transformers at low input voltages. As a result, the new isolator not only meets the stringent requirements of space applications but also offers improved reliability and performance over traditional optocouplers. This advancement represents a significant step forward in the design and implementation of magnetic isolators for use in demanding environments.

Acknowledgment

This work has been financed by the European Space Agency (ESA), under the project High Bandwidth Magnetic Feedback Loop Circuit - ESA Contract No. 4000138724/22/NL/CRS/mkn and the Spanish minister of science, innovation and universities, though the project ”Nuevas topologías para un sistema de distribución secundario estandarizado en satélites” MCIU-22-PID2021-127707OB-C21 and the FPI grant MCINN-23-PRE2022-101790.

REFERENCES

[1] R. A. Reed et al., “Emerging optocoupler issues with energetic particle-induced transients and permanent radiation degradation,” IEEE Trans. Nucl. Sci., vol. 45, n.o 6, pp. 2833-2841, Dec. 1998.

[2] A. H. Johnston, R. D. Harris, y T. F. Miyahira, “Optocouplers: Fundamentals and Hardness Assurance for Space Applications,” IEEE Trans. Nucl. Sci., vol. 56, n.o 6, pp. 3310-3317, Dec. 2009.

[3] K. A. LaBel, A. H. Johnston, J. L. Barth, R. A. Reed and C. E. Barnes, ”Emerging radiation hardness assurance (RHA) issues: a NASA approach for space flight programs,” IEEE Transactions on Nuclear Science, vol. 45, no. 6, pp. 2727-2736, Dec. 1998.

[4] Bob Mammano, “Isolating the Control Loop”. UNITRODE, 1990.

[5] P. K. Rampelli, R. Deekshit, D. S. Reddy, B. K. Singh, V. Chippalkatti, y T. Kanthimathinathan, “Multiple-Output Magnetic Feedback Forward Converter with Discrete PWM for Space Application,” 2012 IEEE International Conference on Power Electronics, Drives and Energy Systems (PEDES), Dec. 2012, pp. 1-6.

[6] “The UC1901 Simplifies the Problem of Isolated Feedback in Switching Regulators,” UNITRODE, pp. 13.

[7] “ADuM3190S Datasheet,” Analog Devices.

[8] S. Sabharwal, J. Kaur, y A. Shahi, “Various Current Mirror Topologies: A Survey,” 2022 2nd International Conference on Advance Computing and Innovative Technologies in Engineering (ICACITE), Greater Noida, India: IEEE, Apr. 2022, pp. 504-508.

[9] A. Dauhajre y R. D. Middlebrook, “Modelling and estimation of leakage phenomena in magnetic circuits,” 1986 17th Annual IEEE Power Electronics Specialists Conference, Vancouver, BC, Canada: IEEE, jun. 1986, pp. 213-226.